

RADIAL PULSATIONS IN POLARIS: A SECONDARY SCIENCE APPLICATION OF CHERENKOV TELESCOPES VIA INTENSITY INTERFEROMETRY

KM NITU RAI,^{1,2} PRASENJIT SAHA³, AND SUBRATA SARANGI^{4,5}

¹School of Physics, Indian Institute of Science Education and Research Thiruvananthapuram, Maruthamala PO, Vithura, Thiruvananthapuram 695551, Kerala, India.

²Aryabhata Research Institute of Observational Sciences, Manora Peak, Nainital 263129, India.

³Physik-Institut, University of Zurich, Winterthurerstrasse 190, 8057 Zurich, Switzerland.

⁴School of Applied Sciences, Centurion University of Technology and Management, Odisha-752050, India. and

⁵ Visiting Associate, Inter-University Centre for Astronomy and Astrophysics, Post Bag 4, Ganeshkhind, Pune 411 007, Maharashtra, India.

(Dated:)

Draft version August 14, 2025

ABSTRACT

Ground-based Cherenkov telescopes, although typically inoperative during moonlit nights for gamma-ray observations, offer a valuable opportunity for secondary scientific applications through Intensity Interferometry (II). Recent developments and observations suggest that implementing II instrumentation on existing Imaging Atmospheric Cherenkov Telescopes (IACTs) or the Cherenkov Telescope Array (CTA) can significantly advance optical stellar measurements. Motivated by the resurgence of II efforts over the past two decades, this work presents simulations demonstrating the estimation of stellar parameters for a radially pulsating star, such as Polaris, using either a single telescope or multiple telescopes. For single-telescope simulations, we assume that the photon pixels in the camera are mapped onto four distinct regions of the aperture, generating multiple baselines and enabling enhanced observational plane coverage. These results highlight the potential of Cherenkov telescopes in India for high-resolution optical astronomy during otherwise inoperative periods and offer promising insights into the characterization of bright stellar objects with unprecedented precision.

1. INTRODUCTION

Intensity Interferometry (II), a technique to observe point sources in sky as extended objects using optical telescopes, was proposed and validated by Hanbury Brown and Twiss ([Hanbury Brown et al. 1956a](#)) wherein the authors reported the results of applying this technique to observe Sirius. This technique was subsequently also applied by Hanbury Brown and team at the historic Narrabri Stellar Intensity Interferometer with the then-available photon detectors. By 1974, this team reported the measurement of the angular diameters of 32 stars in the solar neighborhood [Hanbury Brown et al. \(1974\)](#). However, due to the limitations imposed by the speed of the contemporary photon counters, II passed into a period of slumber. In recent years, with fast photon counters available, there has been a resurgence of interest in II. Several experiments and observations have been conducted using Cherenkov Telescopes Array (CTA) as II telescopes, equipped with faster photon counters at VERITAS, MAGIC, HESS and ASTRI array [Acharyya et al. \(2024\)](#); [Abe et al. \(2024\)](#); [Vogel et al. \(2025\)](#); [de Almeida et al. \(2022\)](#). This revival emphasizes a need for renewed efforts to explore the potential of II in India as a valuable technique to observe bright stellar objects in the northern hemisphere using CTA. The similarity in the basic operational procedures of CTA and the proposed II apparatus is noteworthy. Both of the processes involve photon collection (at the objectives of the telescopes) and counting of the photons received at the photon counters placed on the focal planes (as part of the “eye-pieces”) of the objectives. In both the cases, information on the source of the detected radiation is extracted from the correlation between photons

received at the detectors (the photon counters). Then comes the distinction. During the moonlit nights, the operations of IACTs as Cherenkov Radiation detectors for observing the faint Cherenkov Showers produced by high energy cosmic γ -photons in the upper atmosphere are rendered challenging. However, II measurements can be carried out during such nights at least on observable brighter stars or the stars away from the moon’s trajectory. This similarity and the distinctive operational possibility during moonlit nights have enabled the use of IACTs (like VERITAS [Kieda \(2022\)](#)) as II measurement facilities. Upcoming facilities like the ASTRI Mini-Array in Spain also look forward to carrying out II observations [Stefano Vercellone \(2023\)](#) alongside observations of UHE/ VHE γ -ray events.

At the most basic level, II technique involves measurement of the intensity of radiation received from a stellar source (say, a single, binary or multiple star system) by a pair of telescopes separated by a fixed baseline. The intensity is measured by counting photons of a chosen wavelength λ and within a narrow band width $\Delta\lambda$ received at the photon counters placed at the foci of the telescopes. The bandwidth $\Delta\lambda$ corresponds to a frequency bandwidth $\Delta\nu = | -c\frac{\Delta\lambda}{\lambda^2} |$ and to a coherence time $\Delta\tau = 1/\Delta\nu$. The photons received at the photon counters within the coherence time $\Delta\tau$ are considered coherent and correlated to generate the interference patterns. One of the advantages of II is that these signals from the telescopes can be correlated either real time or be saved and correlated off-line later.

The fundamentals of II are rooted in the van Cittert [van Cittert \(1934\)](#) - Zernike [Zernike \(1938\)](#) theorem. From a practical point of view, Hanbury Brown

and Twiss extended their results [Hanbury Brown et al., R. \(1954\)](#); [Hanbury Brown et al. \(1956b\)](#) of measurements carried out on radio stars using radio-frequency detectors to the visible range by suggesting the replacement of a pair of aerials - rf detector - low pass filter sets with a pair of the mirror - photocell sets where the mirrors acted as the light collectors. In recent times, several laboratory experiments examining various aspects of II have been reported [Dravins et al. \(2014, 2015\)](#); [Rai et al. \(2025\)](#).

It is also worthwhile to note a list of merits and limitations of II over its alternative method, namely, the Michelson Interferometry (MI). The major advantage stems from the fact that the strict requirement of coherence, as in MI, is dispensed with. This allows longer baselines enhancing, thereby, the angular resolution of the observation. IACT facilities like VERITAS and H.E.S.S. which are currently used for II use telescopes with diameters ~ 10 m and baselines of ~ 100 - 200 m to achieve angular resolution beyond \sim milli-arc-seconds range. The classical optical telescopes at La Palma and Chile envisage baselines of ~ 2 km or more with potential for unprecedented angular resolutions upto ~ 30 micro-arc-seconds [Instituto de Astrofísica de Canarias \(2024\)](#). Besides, telescopes of comparatively low optical quality with cheaper optics are acceptable in II thus making establishment of such facilities highly cost-effective compared to the demanding Adaptive Optics of MI telescopes. The other issue with ground-based optical observation is that of atmospheric turbulence and II effectively resolves this issue in the following manner: II measurements are based on the second-order coherence function $g^{(2)}(\tau)$, which tracks the intensity correlations over very short time-scales (nanoseconds). This time-scale is much smaller than the typical time-scales (of milliseconds to seconds) of atmospheric turbulences. As the atmospheric turbulence primarily affects the phase of the incoming wavefronts and not the intensities themselves, II measurements are less affected. As far as the issue of image reconstruction of the source is concerned, both MI and II face difficulties due to incomplete (u, v) plane coverage of the interferometric data and other noises and artefacts. In addition, II has the additional disadvantage of loss of phase information. In the case of MI, the deconvolution methods with incomplete (u, v) plane data and methods of noise suppression due to artefacts have reached a stage of well-established direct pipeline. However, the corresponding methods in II are in an evolving stage; but rapid advances are being made thanks to the emerging powerful methods of Machine Learning techniques. Although, Signal-to-Noise Ratio (SNR) in case of II compared to MI has been a matter of concern in recent past, with availability of fast and high-time resolution photon counters and with upcoming facilities like the CTA, this concern would be amply addressed in coming years.

In this article, we present the results of simulation of II observation of Polaris (a Cepheid star) and estimation of its radius parameters. We have two objectives of carrying out this study:

- Validating II as a technique to observe and measure Cepheids
- Persuading the Indian astronomy community to adopt this versatile technique that can not only

augment the current stellar measurement capabilities but can facilitate measurements of very high angular resolution at little or no additional establishment costs as indicated below.

In this context, we have simulated intensity interferometry (II) observations of Polaris using two ground-based gamma-ray facilities in India and have used the data generated from these simulations to carry out Bayesian estimation of radius parameters of Polaris. The two operational gamma-ray facilities in India are considered as;

- a single large Imaging Atmospheric Cherenkov Telescope (IACT) set up similar to the Major Atmospheric Cherenkov Experiment Telescope (MACE)
- and a subset of three telescopes array similar to the TeV Atmospheric Cherenkov Telescope with Imaging Camera (TACTIC).

These simulations are conducted as a demonstration of the secondary science capabilities of these observatories [Yadav \(2009\)](#). The following sections present the procedure and the key outcomes of this study. The section titled Polaris Observation with II details the simulation of both the signal and noise, employing four sub-apertures on a single telescope and three telescopes array. The subsequent section, Estimation of Parameters, focuses on deriving physical parameters of Polaris, including its mean radius and the amplitude of its radial variation. Finally, the Discussion section compares outcomes from both telescope configurations and discusses the potential role of such Cherenkov telescopes in advancing II-based astronomical studies in India.

2. POLARIS OBSERVATION WITH II

Polaris, also known as Alpha Ursae Minoris (α UMi), is a triple star system located in the northern sky. The primary component, Polaris Aa, forms a close binary with Polaris Ab, separated by approximately 0.17 arcseconds [Evans et al. \(2008\)](#). The third component, Polaris B, orbits this inner binary at a projected separation of about 18 arcseconds [Roemer \(1965\)](#). Polaris Aa, commonly referred to as Polaris, is one of the nearest Cepheid variable stars and lies nearly aligned with Earth's rotational axis, appearing almost stationary in the night sky relative to other stars. Despite its proximity, several aspects of this star remain mysterious, particularly due to the uncertainties in its distance, which have led to discrepancies in the determination of its physical parameters [Van Altena et al. \(1995\)](#); [Turner et al. \(2012\)](#); [Nordgren et al. \(2000\)](#); [Merand et al. \(2006\)](#).

One of the enduring mysteries of Polaris Aa is its pulsating nature. Despite extensive study, the star's fluctuating period and its brightness variation - centered around an apparent magnitude of 1.98 - remain poorly understood. The variability of Polaris has been monitored since 1911, following its confirmation by Ejnar Hertzsprung [Hertzsprung \(1911\)](#). However, the pulsation mode of Polaris remains a subject of debate, primarily due to its small and erratic amplitude variations over time [Usenko et al. \(2018\)](#). While some studies suggest that Polaris pulsates in the fundamental mode, others propose that it may be oscillating in its first or second overtone [Bono et al. \(2001\)](#).

Accurately constraining its pulsational characteristics is crucial not only for the field of asteroseismology but also for refining the calibration of the Cepheid period-luminosity relation, which is instrumental in extragalactic distance measurements. These unresolved issues motivate the choice of Polaris Aa as the subject of this case study, particularly in the context of exploring its observability with Indian optical telescopes using the technique of Intensity Interferometry (II).

We assume that Polaris Aa undergoes a simple harmonic radial pulsation following its fundamental mode, which we model using a simple trigonometric relation. The prior distributions required for the Bayesian estimation are generated using synthetic observation data, based on hypothetical light collectors (or “light buckets”) with dimensions similar to those of MACE and TAC-TIC. The ground coordinates of the modeled mirrors are chosen to match the geographical locations of these two facilities.

2.1. The Photon Flux of Polaris

Let the simple harmonic radial pulsation of the star with its radius $R(t)$ at time t be given by

$$R(t) = R + R_1 \sin\left(\frac{2\pi}{P} t\right) + R_2 \cos\left(\frac{2\pi}{P} t\right) \quad (1)$$

where P is the period of the pulsation, R is the mean radius, and R_1 and R_2 are the oscillatory coefficients in the variation of the mean radius.

It is needless to state that the true variability or pulsation of Cepheid stars is more intricate than a simple harmonic one. However, in the absence of real observational data which could be obtained by using telescopes, we have considered the variations to be of the simplest form. We wish to emphasize that potential to estimate the parameters of more complex functions associated with this variability exists.

Assuming Polaris Aa to be a black body with an average uniform surface temperature T located at a distance D from the observatory and in the direction Ω , the total photon flux reaching the ground from the star at frequency ν at any time t can be expressed as

$$\Phi(\Omega, T) = |S(\Omega, T)|^2 \pi (R/D)^2 \quad (2)$$

where the photon flux in one spectral channel coming from the direction Ω is given by (explained broadly in sec.2.1 of Saha (2020))

$$|S(\Omega, T)|^2 = \frac{\nu^2/c^2}{e^{h\nu/kT(\Omega)} - 1}. \quad (3)$$

having unit photons $\text{m}^{-2}\text{s}^{-1}\text{sr}^{-1}\text{Hz}^{-1}$ and $T(\Omega)$ being the temperature map of the surface of the star whose average value is T .

For a photon detector with bandwidth $\Delta\nu$, the photon flux coming from the source is

$$\Phi(\Omega, T) \Delta\nu = \Phi(\Omega, T) \times \frac{c}{\lambda^2} \Delta\lambda \quad (4)$$

where, λ is the mean observing wavelength around the bandwidth of $\Delta\lambda$.

Fig. 1 shows the spectral distribution of photon flux reaching the ground from Polaris Aa in the bandwidth

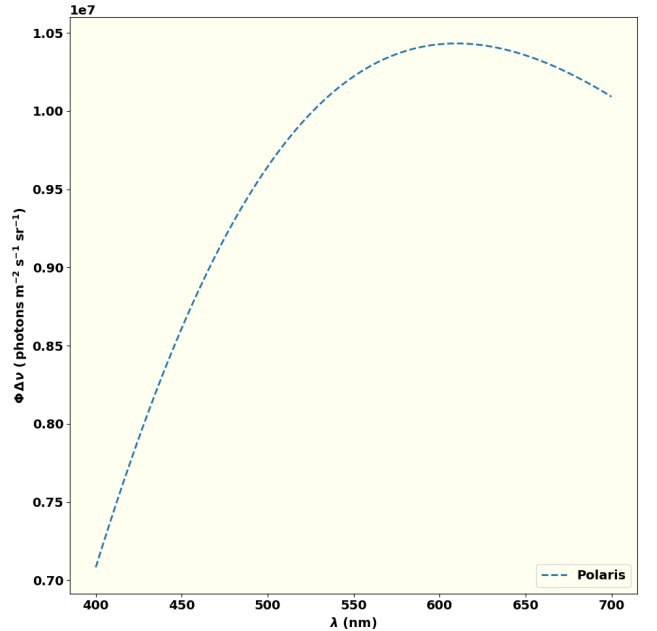


FIG. 1.— The photon flux from a source Polaris in the optical range, while considering the bandwidth of photon detectors $\Delta\lambda = 1\text{nm}$ and mean observation wavelength $\lambda = 570\text{nm}$.

$\Delta\lambda = 1\text{nm}$. The distance of the star from Earth is assumed to be $D = 1 \times 10^{10}$ lightsecond and the average radius of the source at time t is taken to be $R = 87.02$ lightsecond. For the mean observational wavelength $\lambda = 570\text{nm}$ and bandwidth $\Delta\lambda = 1\text{nm}$, the total photon flux is around 1×10^7 photons $\text{m}^{-2}\text{s}^{-1}\text{sr}^{-1}$, which is a good photon statistics for Intensity Interferometry to resolve objects.

2.2. The Signal and Noise for a Baseline

The variation in radius of the star with time is accompanied by variation in its surface temperature; and, as a result the brightness (luminosity) of the star also varies. However, we assume an average surface temperature of the star during the variation cycle of its radius. With this assumption, the visibility signal for a baseline ($u = x/\lambda$, $v = y/\lambda$) on the plane of observation for a single star at a distance D is given by

$$V(\theta, \rho) \propto \frac{J_1(\rho\theta)}{(\rho\theta)} \quad (5)$$

where $\theta = R(t)/D$ is the angular size of star, and $\rho = \sqrt{u^2 + v^2}$ and $J_1(\rho\theta)$ is the Bessel Function of the first kind providing the Airy’s disk intensity distribution due to the star on the ground.

Instead of measuring the complex visibility signal, II measures the squared magnitude $|V(\theta, \rho)|^2$ (or the “squared visibility”) of the signal. As a consequence, the phase information is lost. However, the information about the shape and structure of the source can still be extracted from the squared visibility of the signal. From a practical point of view, we note that a pair of photon detectors fitted at the foci of their respective telescopes measure the intensities $I_1(\theta, \rho)$ and $I_2(\theta, \rho)$ simultaneously. The second-order correlation function

$$g^{(2)}(\theta, \rho) = \frac{\langle I_1(\theta, \rho) \cdot I_2(\theta, \rho) \rangle}{\langle I_1 \rangle \cdot \langle I_2 \rangle} \quad (6)$$

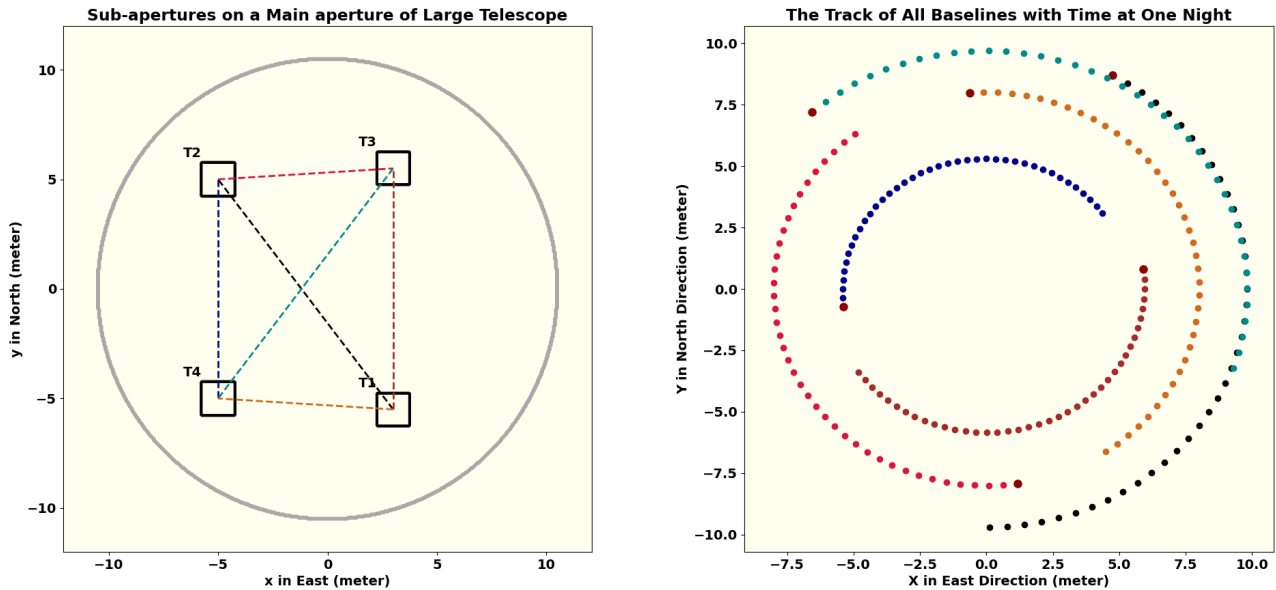


FIG. 2.— On the left, the positions of a set of four small apertures (rectangle shape in black color) on the main aperture (circular shape in brown color) of a telescope are shown. The detectors at the telescope’s focus receive signals only from the area covered by these four sub-apertures. The right panel illustrates the observational coverage during one night using these six sub-apertures.

is computed by a correlator. Then the square magnitude of visibility function and the second order correlation function are related by

$$g^{(2)}(\theta, \rho) - 1 = \frac{\Delta f}{\Delta \nu} |V(\rho, \theta)|^2. \quad (7)$$

We can now define the signal S in terms of the “HBT correlation”, first suggested by Hanbury Brown and Twiss,

$$S = g^{(2)}(\theta, \rho) \propto \frac{\Delta \tau}{\Delta t} |V(\theta, \rho)|^2 \quad (8)$$

where $\Delta \tau$ is the coherence time of the observed radiation and Δt is the temporal resolution of the photon detectors. This equation is used to fit the model of stellar structure. The information on $R(t)$ is extracted using Bayesian methods and the estimates of the mean radius and the parameters responsible for variations in it are inferred (as shown in Rai et al. (2021)).

An observed signal is always accompanied with noise. In fact, in a simulation, where noise also has to be modelled, it can be purposefully designed. The noise N that accompanies the signal S collected from a telescope of effective area A in our simulation is

$$N = (A \Phi \eta n)^{-1} \sqrt{\frac{\Delta t}{t_{av}}} (\text{channels} \times \text{length of observation})^{-1/2} \quad (9)$$

where Φ is the total photon flux from the star (according to equ.2), n is the loss in system, Δt and η are the photon detector’s resolution time and its quantum efficiency respectively. t_{av} is the average observational time over which the the raw time-series data $I_1((\theta, \rho))$ and $I_2((\theta, \rho))$ are smoothed by taking running-averages. The randomness in the noise N (which may arise from several factors such as system loss n , photon flux Φ , effective telescope area A etc.) is factored in through Gaus-

sian sampling. According to eqn. 9, the noise decreases with the number of channels used in observation and the length of observation (ref Fig.9 of Rai et al. (2022) for illustration of this point). Considering it and in search of a good signal-to-noise ratio (SNR) to estimate the complex parameters of stellar objects, we extend the simulation for a longer observational time, typically spanning several hours each night and for several nights. Two primary factors contribute to variations in the visibility signal (equation 5) for Polaris-type variables:

- The change in angular size θ of the star, as described by equation 1.
- and the Earth’s rotation, which plays a significant role in altering the projection of the baseline (u, v) concerning the source. We next discuss the effects of the Earth’s rotation on the baseline.

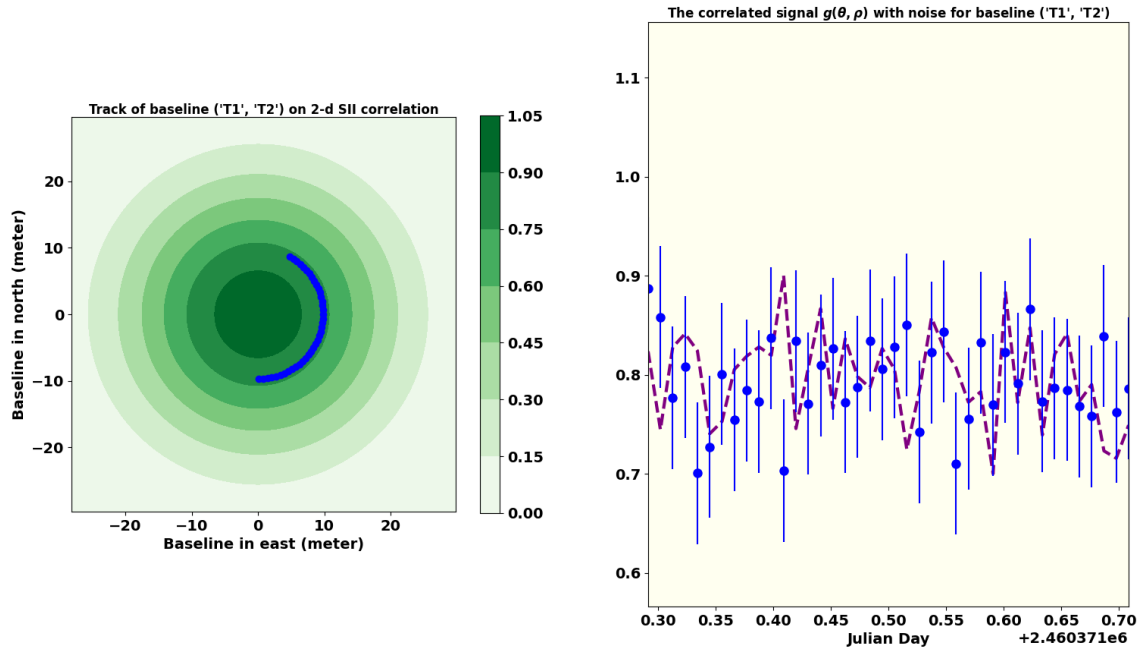
2.3. Rotation of Baseline

The simulated signal from any stellar source observed over long hours overnight has to be modulated with the effect of the rotation of the Earth. This modulation is built into the interferometric coordinates (u, v, w) corresponding to the fixed baseline vector $(\Delta_E, \Delta_N, \Delta_{up})$ associated with a pair of telescopes on the ground using three rotation matrices as shown in eq.(10):

$$\begin{pmatrix} u \\ v \\ w \end{pmatrix} = \frac{1}{\lambda} R_1(\delta) R_2(h) R_1(-l) \begin{pmatrix} \Delta_E \\ \Delta_N \\ \Delta_{up} \end{pmatrix} \quad (10)$$

Here, (u, v) is the baseline vector components in the east and north directions, and w is the perpendicular coordinate along the line of sight to the star (Polaris Aa). The rotation matrices are constructed with the latitude l of the setup, the declination δ and the hour angle h of the

On the observational interval 1



On the observational interval 15

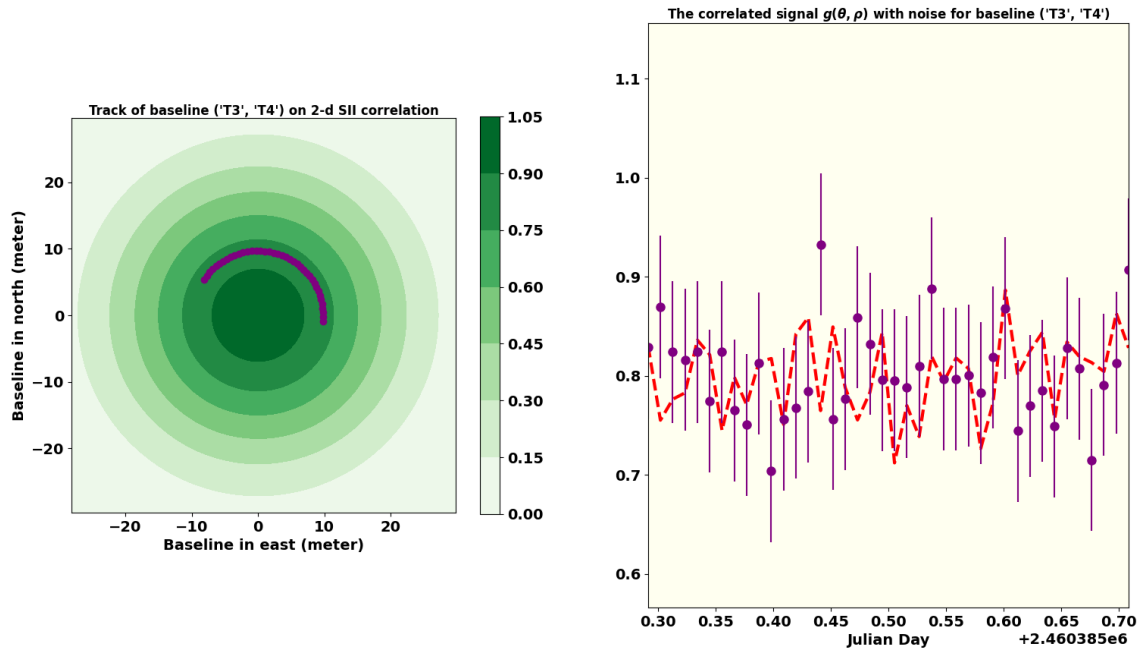


FIG. 3.— The left panels show the baseline tracks created from a single telescope with dense dotted lines on the observational plane, which is filled with the Airy disc of Pulsating Polaris during two observational intervals - day 1 and day 15. The right panel corresponds to simulated intensity interferometry signals plotted against Julian Day. The dotted line with error bars represents the signal assuming the oscillatory (pulsating) nature of Polaris, while the dashed line corresponds to a static (non-pulsating) source. Since the data shown represents a single night's observation, the periodic variability - assumed to have a period of approximately four days - is not clearly visible.

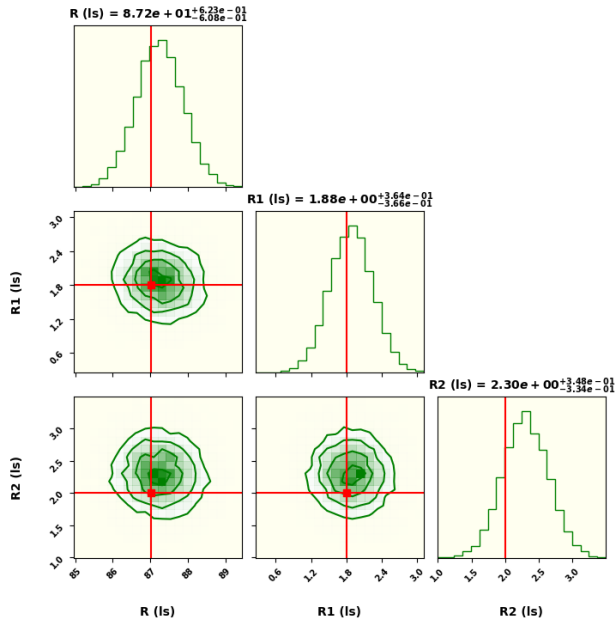


FIG. 4.— It shows the estimated mean radius and maximum radial variation of Polaris derived from simulated single telescope observations over 15 days each with 10 hours.

source according to

$$R_1(\delta) = \begin{pmatrix} 1 & 0 & 0 \\ 0 & \cos \delta & -\sin \delta \\ 0 & \sin \delta & \cos \delta \end{pmatrix}, \quad (11)$$

$$R_1(l) = \begin{pmatrix} 1 & 0 & 0 \\ 0 & \cos l & -\sin l \\ 0 & \sin l & \cos l \end{pmatrix}, \quad (12)$$

and

$$R_2(h) = \begin{pmatrix} \cos h & 0 & \sin h \\ 0 & 1 & 0 \\ -\sin h & 0 & \cos h \end{pmatrix}, \quad (13)$$

In the upcoming section, we will see that these three matrices will be applied according to the position of the telescope with respect to the source. It is to be noted that, the latitude l of the observatory and declination δ of the observed source being constant, the time variation in the (u, v, w) coordinates results from the time variation $h(t)$ of the hour-angle of the source during the observation.

3. A SINGLE LARGE IACT

We simulate a single telescope, which is located at Hanle, Ladakh, India, at an altitude of 4270 meters above sea level. It is a large Imaging Atmospheric Cherenkov Telescope (IACT) featuring a 21-meter diameter reflector composed of 1424 mirror facets, each measuring approximately $0.5 \text{ m} \times 0.5 \text{ m}$ in size, similar to Major Atmospheric Cherenkov Experiment Telescope (MACE) [Bhatt et al. \(2021\)](#). The high-altitude location, large aperture, and optical quality make it a promising candidate for applications in Intensity Interferometry (II). However, with only a single telescope, one is limited to measuring zero-baseline intensity correlations, and this restricts spatial resolution. Multiple baselines are essential to capture interference fringes to retrieve detailed

information about the source structure and morphology. Even so, the substantial aperture of it with tessellated mirror facets offers possibilities of implementing the “split mirror technique” and emulating multiple baselines. This can be implemented by configuring sub-apertures consisting of a group of contiguous mirror facets across their surface. Using groups of such sub-apertures located at fixed distances with respect to each other on the surface of the objective of the telescope, the study of spatial coherence and improving the angular resolution of stellar objects can be achieved by carrying out II observation and evaluating HBT correlation. We discuss the simulation of the II observation of Polaris with implementation of the “Split Mirror Technique” on the telescope below.

3.1. A Split Mirror Technique with a Single Telescope

In this study, we consider an observational configuration in which a block of nine neighbouring mirror facets, each with approximately identical focal lengths, is grouped into a square panel measuring $1.5 \text{ m} \times 1.5 \text{ m}$. These panels represent a modular sub-aperture unit of the telescope. As illustrated in the left panel of Figure 2, our simulation utilizes the signal collected from four such mirror panels (represented by the four small rectangular shapes) distributed at distinct positions on the circular primary reflector (circular shape in brown color) of the telescope. In this configuration, the photo-detector assembly of the telescope’s imaging camera is restricted to receiving light exclusively from these four spatially separated sub-apertures. This method, known as the split-mirror technique, enables the creation of multiple virtual baselines, which are essential for intensity interferometry (II). These virtual baselines mimic the effect of physically separated telescopes, thereby enhancing the spatial sampling of the source’s brightness distribution. The right panel of Figure 2 depicts the tracks traced by the six possible baselines formed due to Earth’s rotation between the four panels during a single night of observation. In each track, the dark red dot marks the endpoint of the baseline trajectory, while the tail indicates the start of the observation. While this figure shows the coverage for one night, multiple nights of observation are typically accumulated to improve the signal-to-noise ratio (SNR) and achieve reliable II measurements.

The noise associated with the simulated signal is computed using the expression defined in Equation 9. This expression incorporates contributions from the total photon flux, instrumental characteristics of the telescope, and observational parameters. For calculating the photon flux, Polaris is assumed to have an average surface temperature of 6015 K. The resolution time of the photon detectors is taken as $\Delta t = 1 \text{ ns}$, and each observation session spans 15 minutes. The simulation assumes a single detection channel and a total observational duration of 15 nights each for 10 hours. In this simulation, the quantum efficiency of the photon detector (η) and the signal loss factor (n) are both assumed to be unity, i.e., $\eta = 1$ and $n = 1$, to focus on the theoretical limit. The effective light-collecting area for each set of four mirror facets is taken as $A = 2 \text{ m}^2$. Under these conditions, the total signal-to-noise ratio (SNR) achieved over 15 nights of observation is approximately 1165. This SNR is sufficiently high to reliably estimate both the average radius

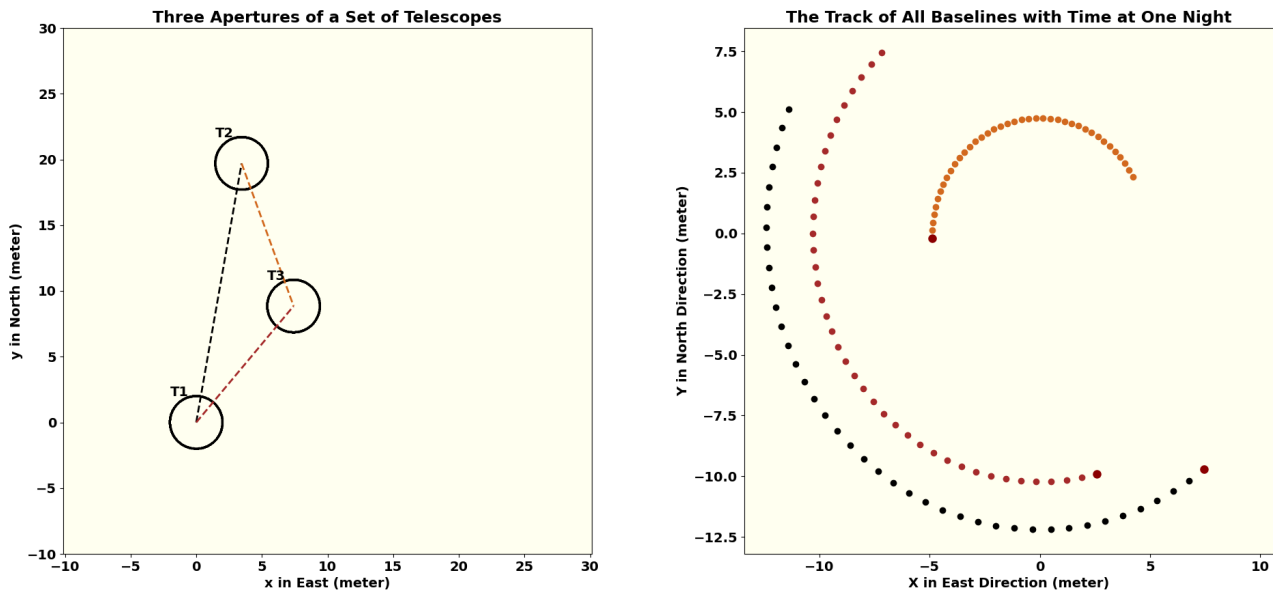


FIG. 5.— The left panel shows the positions of three selected telescopes array. The detectors used in these telescopes are photomultiplier tubes (PMTs). Right panel visualizes the observational coverage for a single night based on the baselines formed by the selected telescopes.

and its variation for Polaris. Notably, the determination of only the mean radius does not require such a high SNR, implying that even shorter observation durations could be acceptable for certain objectives.

3.2. The Signal and Estimation of Parameters

Figure 3 presents the results of simulated observations for a single night. The left panel displays a contour map of the HBT correlation signal over a specific time interval (averaged over a few minutes). Superimposed on this plot are the baseline tracks traced by telescope pairs (T1, T2) and (T3, T4) due to Earth’s rotation, indicated by dense dotted lines.

The right panel of the figure shows the correlated signal as a function of Julian Day for the tracked baselines. Two simulated signals are presented: one assuming Polaris exhibits oscillatory radial variation (plotted as dotted lines with error bars) and the other assuming a static nature of the star (shown as a dashed line). Since the observation is limited to one night, the periodic pattern corresponding to Polaris’s pulsation, assumed to have a period of four days, is not yet visible in the data.

To estimate stellar parameters, we simulate a longer observational campaign spanning 15 nights. Using the nested sampling algorithm implemented in *dynesty* [Speagle \(2020\)](#), we infer the oscillatory characteristics of Polaris under the assumption of radial pulsation. The results are presented in Figure 4. With a sufficiently high signal-to-noise ratio achievable using a single large telescope, the mean stellar radius (R) and the amplitudes of its oscillation (R_1 and R_2) are estimated with uncertainties of approximately 0.71%, 19.30%, and 15.26%, respectively. This successful estimation of the three parameters strongly suggests that real-time observation be mounted using a single telescope. Such observations would enable testing of more complex oscillation models of Polaris and other Cepheids.

4. THREE SETS OF IACTS ARRAY

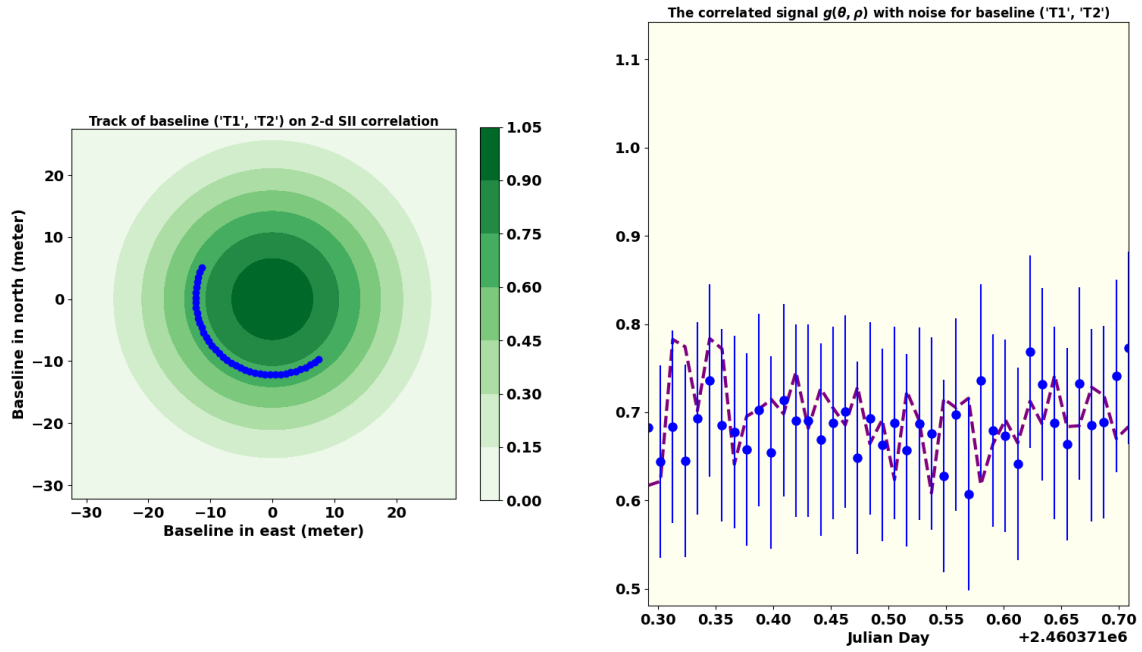
We simulate a ground-based gamma-ray observatory consisting of three telescope arrays similar to the TeV Atmospheric Cherenkov Telescope with Imaging Camera (TACTIC) located at Mount Abu, Rajasthan, India. TACTIC represents India’s first imaging atmospheric Cherenkov telescope (IACT) dedicated to very high-energy (VHE) gamma-ray astronomy. The TACTIC array comprises four telescopes: three positioned at the vertices of an equilateral triangle with a side length of approximately 20 meters and one located at its centroid [Tickoo et al. \(1999\)](#).

We assume the geometric configuration and the high instrumental precision similar to TACTIC, which makes the three telescopes used in this study a promising candidate for Intensity Interferometry (II) observations. The arrangement of telescopes ensures a well-distributed coverage across the observational plane, enabling effective photon correlation measurements. For our simulation, we consider only three of the telescopes in the array, as illustrated in Figure 5. Each telescope is constructed using 34 circular mirror facets, each 0.6 m in diameter, yielding a total effective light-collecting area of approximately 9.5m^2 per telescope [Koul et al. \(2007\)](#).

4.1. Three Telescopes of an Array and the Signal as II

To investigate the oscillatory behavior of Polaris using Intensity Interferometry (II), we consider three telescopes from an array, as depicted in the left panel of Figure 5. Each telescope is equipped with a photomultiplier tube (PMT) featuring a time resolution of 3 ns. The right panel of the figure illustrates the tracking of all three baselines formed by this configuration, plotted in the same format as for the single telescope in Figure 2. The instrumental characteristics of these telescopes are incorporated into the signal simulation. Only 20% of each aperture’s area is considered to account for

On the observational interval 1



On the observational interval 1

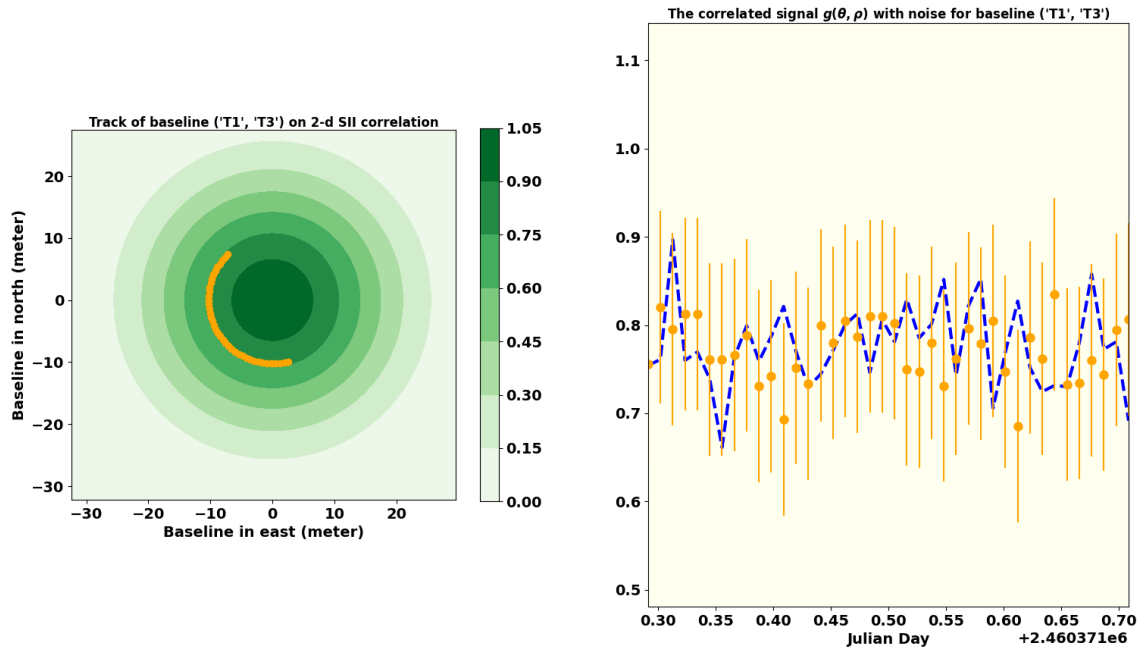


FIG. 6.— The left panels show the airy pattern of oscillatory Polaris. The blue and yellow densely dotted lines represent the tracking of the Airy pattern over one night of observation along the base lines (T1, T2) and (T1, T3) (as shown in Fig. (5)). The right panels correspond to the simulated signals plotted against Julian Day. Two signal types are shown - one representing the oscillatory nature of Polaris (dotted lines with error bars) and the other representing a static model (dashed lines), as also depicted in Figure 3.

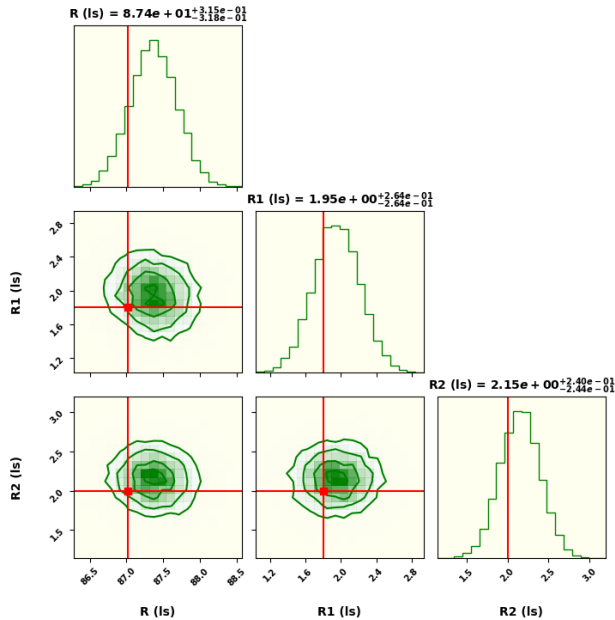


FIG. 7.— The estimated value of Polaris’s mean and maximum variable radius with three telescope array.

system inefficiencies such as quantum efficiency and signal loss, resulting in an effective photon-collecting area of approximately 2m^2 per telescope. While the mean radius of Polaris can be inferred from a shorter observation period, accurately estimating the maximum radius variation requires a high signal-to-noise ratio (SNR), so a long observational length is needed. To achieve this, we simulate 15 nights each with 10 hours of observation using two channels, yielding an SNR of approximately 1050. Alternatively, the same SNR can be achieved with a single channel over 30 nights. Since only three baselines are formed with the selected telescopes, two of these baselines are visualized in Figure 6 for a single night of observation. The left panel shows the simulated II signal as a green contour map, along with the tracking of baselines marked by dense dotted lines. The right panel presents the extracted signal from these tracks, highlighting the distinction between Polaris’s oscillatory (dotted with error bars) and static (dashed line) models.

4.2. The Parameter Estimation with Three Arrays

The signal strength depicted in the right panel of Figure 6 demonstrates sufficient quality to recover the simple trigonometric parameters associated with the pulsating model of Polaris (Eqn. 1). Using simulated data from the three-telescope configuration, we estimated the mean radius R and the amplitudes R_1 and R_2 of its variation. The results, presented in Figure 7, indicate that the mean radius R of Polaris is determined with an uncertainty of approximately 0.36%. The oscillatory parameters, R_1 and R_2 are estimated with 13.58% and 11.11% uncertainty respectively. Notably, these uncertainties are lower than those obtained using the single telescope simulation (see Figure 4), suggesting improved parameter

constraints with the three-telescope configuration. However, it is important to note that in the three-telescope simulation, two detection channels were used to reduce noise, whereas only one channel was considered in the single-telescope simulation. Conversely, the single telescope configuration benefits from six baselines using the split mirror technique, providing stronger spatial coverage compared to the three baselines available with the array.

5. CONCLUSION

The resurgence of Intensity Interferometry (II) as a technique for high-resolution stellar imaging has been significantly driven by its adoption during moonlit nights by major Cherenkov Telescope Arrays (CTA) and Imaging Atmospheric Cherenkov Telescopes (IACTs). The combination of large collecting apertures and long baselines makes these facilities particularly well-suited for II, offering the signal-to-noise ratios necessary to resolve fine details in stellar structures at optical wavelengths. Recent advancements by facilities such as VERITAS, MAGIC, HESS, and the ASTRI array have demonstrated the feasibility of using II for the angular resolution of complex stellar systems, including OB-type stars, Wolf-Rayet stars, and pulsating stars in binaries and multiple systems Acharyya et al. (2024); Abe et al. (2024); Vogel et al. (2025); de Almeida et al. (2022).

In this work, we have explored the secondary science potential of Indian Cherenkov facilities - specifically similar to the MACE and the TACTIC observatory - for II observations. Using Polaris as a test case, we have successfully simulated two separate II observation campaigns using these telescopes and have estimated its mean radius and oscillatory behavior with good precision. The results indicate that even with a limited number of baselines and modest instrumental configurations, valuable astrophysical parameters can be extracted.

These findings not only highlight the feasibility of utilizing Indian IACTs for II during non-gamma observational periods, such as moonlit nights, but also strongly suggest that real-time collaborative efforts be undertaken using these existing Indian facilities. At very little or no additional costs, Indian marks would be made in this prospective and resurging field of Astronomy. Moreover, the success of this approach points toward a broader potential: other optical telescopes with sensitive photon detectors at the focus may also be adapted for II applications. Looking forward, the extension of this method beyond the northern sky, combined with collaborative efforts involving southern hemisphere facilities, promises to open a new era of high-resolution optical astronomy.

Acknowledgment: One of the authors (SS) gratefully acknowledges the computing facilities and the local hospitality extended to him by the Inter-University Centre for Astronomy and Astrophysics (IUCAA), Pune, India under its Visiting Associate Programme during the preparation of this manuscript.

REFERENCES

- Bono, G., Gieren, W., Marconi, M., & Fouqué, P. 2001, *The Astrophysical Journal*, 552, L141
- de Almeida et al., E. S. G. 2022, *Monthly Notices of the Royal Astronomical Society*, 515, 1
- Dravins et al., D. 2014, in *Optical and Infrared Interferometry IV*, Vol. 9146, SPIE, 298–315
- Dravins et al., D. 2015, *Astronomy & Astrophysics*, 580, A99
- Evans et al., N. R. 2008, *The Astronomical Journal*, 136, 1137
- Hanbury Brown et al., R. 1956a, *Nature*, 178, 1046
- Hanbury Brown et al., R. 1956b, *Nature*, 177, 27
- Hanbury Brown et al., R. 1974, *Monthly Notices of the Royal Astronomical Society*, 167, 121
- Hanbury Brown et al., R. 1954, *Philosophical Magazine*, 45, 663
- Hertzprung, E. 1911, *Astronomische Nachrichten*, volume 189, Issue 6, p. 89, 189, 89
- Instituto de Astrofísica de Canarias. 2024, The LPI project will explore new frontiers of quantum astronomy in La Palma
- Kieda, D. B. 2022, in *Optical and Infrared Interferometry and Imaging VIII*, Vol. 12183, International Society for Optics and Photonics (SPIE), 121830D
- Koul et al., R. 2007, *Nuclear Instruments and Methods in Physics Research Section A: Accelerators, Spectrometers, Detectors and Associated Equipment*, 578, 548
- Merand et al., A. 2006, *Astronomy & Astrophysics*, 453, 155
- Nordgren et al., T. E. 2000, *The Astrophysical Journal*, 543, 972
- Rai, K. N., Basak, S., Sarangi, S., & Saha, P. 2025, *Resonance*, 30, 45
- Rai et al., K. N. 2021, *Monthly Notices of the Royal Astronomical Society*, 507, 2813
- Rai et al., K. N. 2022, *Monthly Notices of the Royal Astronomical Society*, 516, 2864
- Roemer, E. 1965, *Astrophysical Journal*, vol. 141, p. 1415, 141, 1415
- Saha, P. 2020, The theory of intensity interferometry revisited
- Speagle, J. S. 2020, *Monthly Notices of the Royal Astronomical Society*, 493, 3132
- Stefano Vercellone. 2023 [2302.10000]
- Tickoo et al., A. 1999, *Experimental Astronomy*, 9, 81
- Turner et al., D. G. 2012, *The Astrophysical Journal Letters*, 762, L8
- Usenko et al., I. 2018, *Monthly Notices of the Royal Astronomical Society: Letters*, 481, L115
- Van Altena et al., W. 1995, *VizieR Online Data Catalog*, I
- van Cittert, P. 1934, *Physica*, 1, 201
- Vogel et al., N. 2025, *Monthly Notices of the Royal Astronomical Society*, 537, 2334
- Yadav, K. K. 2009, TACTIC and MACE gamma-ray telescopes
- Zernike, F. 1938, *Physica*, 5, 785